An improved understanding of fatigue crack growth behavior of multiple collinear cracks in hybrid composite structures

Wang, Wandong; Zhao, Hongchen; Zhang, Zhinan; Sun, Wenbo; Rans, Calvin; Ma, Yu'e

DOI
10.1016/j.ijfatigue.2025.108997

Publication date
2025

Document Version
Final published version

Published in
International Journal of Fatigue

International Journal of Fatigue 198 (2025) 108997

Contents lists available at ScienceDirect

International Journal of Fatigue

journal homepage: www.elsevier.com/locate/ijfatigue

An improved understanding of fatigue crack growth behavior of multiple collinear cracks in hybrid composite structures

Wandong Wang [a,b], Hongchen Zhao [a], Zhinan Zhang [a,c], Wenbo Sun [a,b,*], Calvin Rans [d], Yu'e Ma [a,b]

[a] School of Aeronautics, Northwestern Polytechnical University, 710072, Xi'an, Shaanxi, PR China
[b] National Key Laboratory of Strength and Structural Integrity, Northwestern Polytechnical University, 710072, Xi'an, Shaanxi, China
[c] Department of Strength Design, AVIC the First Aircraft Institute, Xi'an, 710089, China
[d] Faculty of Aerospace Engineering, Delft University of Technology, Kluyverweg 1, Delft, 2629 HS, The Netherlands

ARTICLE INFO

Keywords:
Fiber–metal laminates
Multiple collinear fatigue cracks
Crack acceleration
Limit of validity
Stress intensity factor

ABSTRACT

Accurately predicting MSD crack growth behavior in hybrid metal–composite structures is challenging due to the complex interactions of fiber bridging and delamination failure in fiber–metal laminates (FMLs). These mechanisms enhance damage tolerance but complicate crack analysis. This paper proposes two analytical models to address crack growth in FMLs with multiple collinear cracks. The first model analyzes crack openings and stress intensity factors (SIFs) for multiple cracks, capturing the physics of MSD cracking, but it is cumbersome to implement. The second model simplifies the problem by considering energy dissipation, treating the MSD scenario as a single crack in a finite plate and equating the energy dissipation between both cases. Both models were validated and show accurate predictions of crack growth behavior, capturing crack acceleration effectively. The results emphasize the importance of accounting for the contributions of bridging and stiffening mechanisms in FMLs, particularly load redistribution, which influences crack growth.

1. Introduction

The damage tolerance philosophy is a cornerstone of aerospace engineering, ensuring structural integrity by designing structures to withstand and safely accommodate damage such as fatigue cracks until detected and repaired [1,2]. This design philosophy prioritizes safety through inspections and maintenance while allowing for potential weight saving. Bonded built-up aerospace structures are therefore favored owing to their superior damage tolerant properties. The externally bonded strengthening elements, such as stringers, tear straps and repair patches, can significantly retard the fatigue crack growth in skin panels [3,4].

Alternatively, interleaving thin metal layers and fatigue-resistant fiber layers using bonding techniques creates Fiber–Metal Laminates (FMLs), a family of hybrid composites well-suited to complement the damage tolerance philosophy [5,6]. The fibers remain intact in the event of fatigue cracking in the metal layers, effectively restraining crack opening and significantly reducing the stress intensity factor at the crack tips. In addition to their exceptional fatigue resistance, FMLs exhibit superior impact resilience, corrosion resistance, and other advantageous properties [7]. Consequently, FMLs have been widely adopted in high-performance applications across aerospace engineering, automotive, wind energy, and other industrial sectors [8,9].

While the damage tolerance philosophy has demonstrated great effectiveness, a notable limitation lies in its lack of constraints on service life [10]. This gap raises the risk of widespread fatigue damage (WFD) in aging aircraft, typically characterized by the simultaneous presence of multiple cracks within a structural element [11,12]. To address this issue, airworthiness regulations introduced the Limit of Validity (LOV) concept. The LOV establishes a defined operational life, beyond which the occurrence of WFD is not anticipated [13]. This regulatory shift merits further investigation of multiple site damage (MSD) scenarios in monolithic metal structures and bonded built-up structures.

It is well known that the damage tolerance behavior of monolithic metallic structures [12,14,15], bonded built-up structures [16–18] and hybrid composite FMLs [6,19–23] have been extensively studied. Similarly, the MSD fatigue behavior in monolithic metallic structures has drawn great deal of attention and has been thoroughly studied experimentally [24,25], analytically [26,27], numerically [28,29]. In contrast, research on MSD in hybrid FML composites remains limited [10,30,31], highlighting a gap in the existing body of knowledge.

* Corresponding author at: School of Aeronautics, Northwestern Polytechnical University, 710072, Xi'an, Shaanxi, PR China.
E-mail addresses: w.wang@nwpu.edu.cn (W. Wang), zhaohongchen@mail.nwpu.edu.cn (H. Zhao), zhangzhinan198678@126.com (Z. Zhang), wenbo-sun@nwpu.edu.cn (W. Sun), C.D.Rans@tudelft.nl (C. Rans), ma.yu.e@nwpu.edu.cn (Y. Ma).

https://doi.org/10.1016/j.ijfatigue.2025.108997
Received 12 January 2025; Received in revised form 1 March 2025; Accepted 9 April 2025
Available online 23 April 2025

It is essential to briefly highlight the complexities involved in analyzing the damage tolerance behavior of FMLs before addressing the challenges in predicting their MSD behavior. The fatigue-resistant fibers bridge cracks in the metal layers, redistributing loads and retarding crack growth. However, the cyclic stresses induce delaminations, adding another layer of complexity to failure mechanisms. Predicting the damage tolerance behavior of FMLs relies on analytical models based on linear elastic fracture mechanics (LEFM), the principles of superposition and displacement compatibility [6]. The displacement compatibility between the crack opening and the intact fiber deformation at the delamination front is employed to determine the interplay between cracking in metal layers and delaminations at composite–metal interfaces [32]. These models use stress intensity factors (SIFs) and strain energy release rates (SERRs) to capture the coupled crack and delamination growth, providing insights into the fatigue crack growth behavior of FMLs. The established models fail to capture the crack acceleration of FMLs in the simultaneous presence of MSD cracks, which is attributed to the fact that other cracks cause load redistribution that exacerbates both the SIFs and SERRs [10,31]. Thanks to the redundant load paths in FMLs, the load redistribution mechanism persists throughout the relatively steady crack growth, accelerating the crack growth rate and significantly reducing the overall crack growth life [10,31].

Endeavors have been made to capture the load redistribution and crack growth acceleration by representing the presence of MSD cracks in FMLs as removal of metal strips [10,33]. While this non-physical approach captures crack growth acceleration effectively, the predictions are highly conservative, with errors worsening for FMLs with higher metal volume fractions (MVF). While these models provide a safe baseline, they fail to capture the nuanced interactions between cracks and delaminations, resulting in overly conservative predictions that limit their applicability. An in-depth understanding of the MSD scenario in FMLs and accurate analysis tools are still lacking.

To advance the fine-tuned safety design of hybrid FML composite structures in light of the limitations placed by LOV on the damage tolerance philosophy, a more in-depth understanding of MSD crack growth behavior is necessary. Improved prediction methodologies must account for the subtle load redistribution and coupled failure mechanisms inherent in these materials. This paper focuses on the improved understanding of fatigue crack growth behavior for multiple collinear cracks in hybrid FMLs. Two analytical models are proposed in this paper. One model closely reflects the physics of MSD cracking in FMLs by analyzing the crack openings and SIFs of multiple cracks, and implementing the bridging mechanism over multiple cracks. Another model is a simplification of MSD in FMLs to a finite width problem by following the argument that the fatigue failure energy dissipation of these two scenarios should be equivalent. The two models have been validated to show that both accurately predict the fatigue crack growth life and capture crack acceleration behavior. The fatigue behavior of FMLs closely resembles that of other bonded built-up structures. Both systems exploit redundant load paths and crack retardation mechanisms, such as adhesively bonded reinforcements, to enhance fatigue resistance. Insights gained from studying MSD in FMLs could contribute to safer and more efficient engineering designs of more general built-up bonded structures, reinforcing their utility in safety-critical applications.

2. Analogy between a MSD scenario and a crack in a finite width panel

A row of evenly distributed collinear cracks in a monolithic metallic plate, illustrated in Fig. 1(a), is the most studied MSD case in the open literature. The closed-form solution for the stress intensity factor at the tips of cracks of length $2a$ with a spacing of W under far-field applied stress, σ_{app}, has been well established [34,35]. The exact stress intensity factor at the crack tip is provided in Eq. (1). It is well known that the stress intensity factor soars up as crack tips grow towards each other prior to coalescence.

$$K_{MSD} = \sigma_{app}\sqrt{(W\tan(\frac{\pi a}{W}))} \tag{1}$$

It is of great interest to determine the ratio between the SIF for the evenly distributed collinear cracks scenario and the SIF of a single crack in an infinite plate, $K_{inf} = \sigma_{app}\sqrt{\pi a}$, highlighting the increase in relative magnitude of SIF due to the presence of multiple cracks. The ratio, β_{MSD}, can be defined as in Eq. (2)

$$\beta_{MSD} = \frac{K_{MSD}}{\sigma_{app}\sqrt{\pi a}} = \sqrt{\frac{W}{\pi a}\tan(\frac{\pi a}{W})} \tag{2}$$

A similar phenomenon can be observed in the SIF for a single crack of $2a$ in a plate of W in width as the crack grows towards the free edge. A finite width correction factor, β_{FW}, is normally employed to capture the increase in SIF magnitude, i.e., the SIF for this case is given as $K_{FW} = \beta_{FW}K_{inf}$. Several finite width correction factor solutions have been developed, such as the Isida solution [36], the Dixon solution [37] and the Feddersen solution [35]. Particularly, Irwin [38] provided a finite width correction factor of tangent formula which is identical to Eq. (2).

In Fig. 2, β_{MSD} is compared against several β_{FW} solutions for different $2a/W$ values. As can be seen, they are in good agreement over a wide range of $2a/W$. The underlying physics of this agreement, as shown in Fig. 2, lies in the same cracking phenomenon. Chandran [39] has compared the stress distribution ahead of the crack tip in the MSD scenario against that of a single crack in a finite width panel, based on the Westergaard stress function. The two stress distributions closely overlap with each other and their magnitudes increase as $2a/W$ increases faster than that of a single crack in an infinite plate, as schematically shown in Fig. 1. Chandran has related the increase in SIF to the increase in the stress distribution. Wang et al. [40] have reached the same conclusion by determining the increase in the stress distribution ahead of the crack tip in a finite width panel based on the Westergaard stress function and the force equilibrium between the cracked cross-section and far-field. Zhao et al. [41] have correlated the increase in the SIF with the increase in the applied work and thus the energy dissipation at the crack tip as the crack length increases. They have measured the applied load and the displacement at the loading point to determine the increase in applied work, which has shown great agreement with the finite-width correction factors.

The investigations discussed in the preceding paragraphs shed light on the SIF correlation between the MSD and a single crack in a finite width panel, as depicted in Fig. 1, from the physics point of view. As the crack length increases, the net cross-section decreases, yet it transmits the same amount of far-field applied load. The force equilibrium between the far-field and the cross-section clearly demonstrates an increase in the stress distribution, which can be depicted by the Westergaard stress distribution form, ahead of the crack tip. What is more, the increase in the stress distribution also indicates that the strain distribution is increased according to Hooke's law. The product of the increased stress and strain distribution results in enlarged strain energy, which requires the applied work to increase as well. The SIF of MSD cracks and that of a single crack in a finite width panel shown in Fig. 1 share the same mechanism in terms of the stress distribution and applied work. Chandran [39], Wang et al. [40] and Zhao et al. [41] have examined the problem from different perspectives; however, their approaches converge on the same fundamentals.

It is assumed in this paper that the MSD crack growth behavior in FMLs shares the same crack acceleration behavior as a single crack in an FML panel with finite width, as shown in Fig. 3, analogous to what has been discussed about the crack acceleration in the monolithic metal panel for the MSD and single crack cases. From the energy point of view, as multiple cracks simultaneously grow towards each other, the net cross-section and stiffness of the built-up hybrid panel decreases so

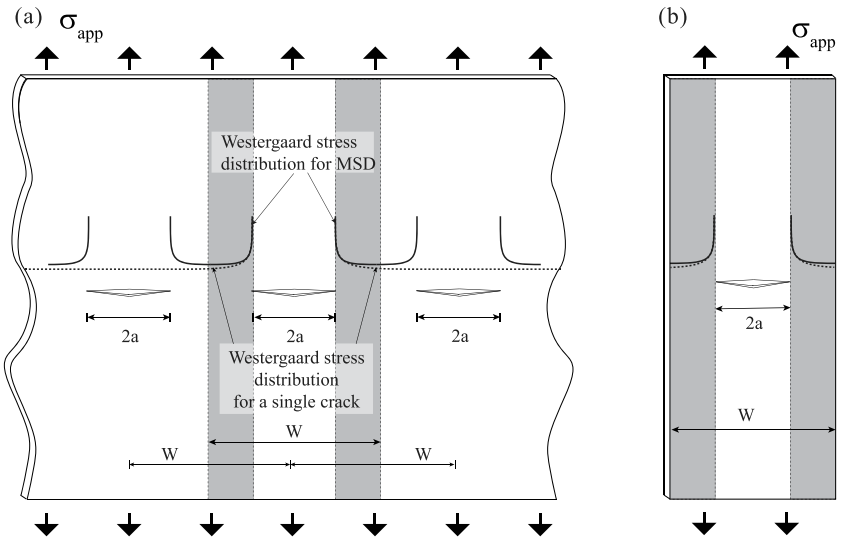

Fig. 1. An analogous comparison between (a) evenly distributed cracks in a panel and (b) a single crack in a finite width panel.

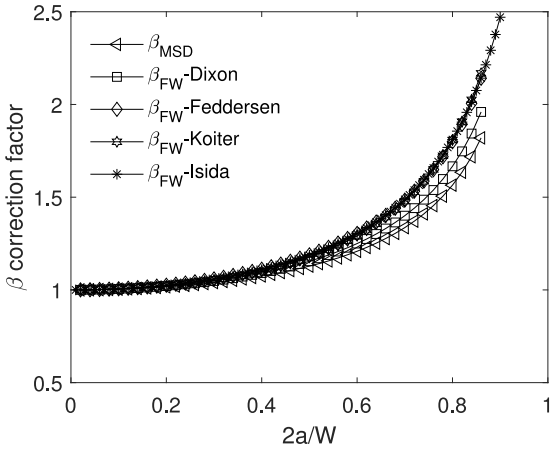

Fig. 2. Comparison between β_{MSD} and several β_{FW} solutions for monolithic metal panels.

that the far-field applied load does more work to the system. The energy dissipation of the crack tip thus increases. This mechanism is assumed to be equivalent to a single crack growth in a finite width FML under the same far-field applied stresses. Zhao and Alderliesten [41,42] have experimentally studied the increase in applied work of a single crack in an FML panel in order to propose an empirical finite width correction factor to capture the crack acceleration behavior. They have found that the crack acceleration behavior is related to the FML grade.

While the mechanism of crack acceleration in an FML is easy to understand, it is difficult to capture the acceleration behavior with prediction models. Unlike for monolithic panels, a similar correction factor cannot be simply and directly applied to the bonded and built-up structures. Wang [43] has developed an analytical model to correct for the finite width effect on the crack acceleration by also accounting for the FML grade and fiber bridging. The fundamental assumption in this paper is that the previously developed model can be used to capture the crack acceleration for the MSD scenario in FML panels with different grades. A reasonable analogy between the MSD effect and the finite width effect should also be provided to deepen our understanding of the fatigue crack growth of multiple collinear cracks in built-up structures.

3. Model development

In this paper, two approaches have been developed to address the interaction of multiple cracks in FMLs with the objective of gaining in-depth insights into the understanding of the MSD fatigue failure behavior. The overall road-map of how fatigue behavior in FMLs can be analyzed is provided first and then the difference in dealing with the interaction or acceleration of MSD cracks is highlighted in the two analytical approaches respectively.

There are two coupled fatigue failure mechanisms in FMLs, i.e., fatigue cracking in the metal layers accompanied by delamination at the interface of metal/fiber layers. The fatigue resistant fibers remain intact and restrain the opening of fatigue cracks in the metal layers under far-field applied loading, as shown in Fig. 4. As a result, partial loads are transferred to the intact fibers via cyclic shear at the metal/fiber interfaces. This so-called bridging mechanism reduces the SIF at the crack tip and renders delamination at the interfaces.

Analytical models have been well established to deal with both the fatigue crack growth and the accompanying delamination propagation for a single crack in an FML [6,19,20,32]. The classic laminate theory is applied to calculate the lamina stresses in the metal layers, σ_m, and in the fiber layers, S_f. The SIF at the crack tip and the SERR distribution along the delamination front need to be determined to predict the crack propagation and delamination growth.

As for the analysis of the cracking in the metal layers, the total SIF, K_{total}, at the crack tip is given in the following equation:

$$K_{total} = K_{ff} + K_{br} \tag{3}$$

with K_{ff} and K_{br} being the SIFs owing to the far-field applied loading and the bridging mechanism respectively. K_{ff} is a function of σ_m and the crack configuration. K_{br} is determined by analyzing the bridging stress distribution based on the principle of displacement compatibility [6,32].

As shown in Fig. 4, it is essential to determine the bridging stresses, $S_{br}(x)$, in order to calculate both K_{br} and the strain energy release rate, $G(x)$, at the delamination front. To achieve this, the delamination shape is discretized into a series of bar elements (Fig. 4). The x-y coordinate system is defined with its origin at the crack center, where the x-axis lies along the crack plane and the y-axis is perpendicular to the crack plane. The principle of displacement compatibility between the metal layer and the fiber layer is implemented at the delamination front for

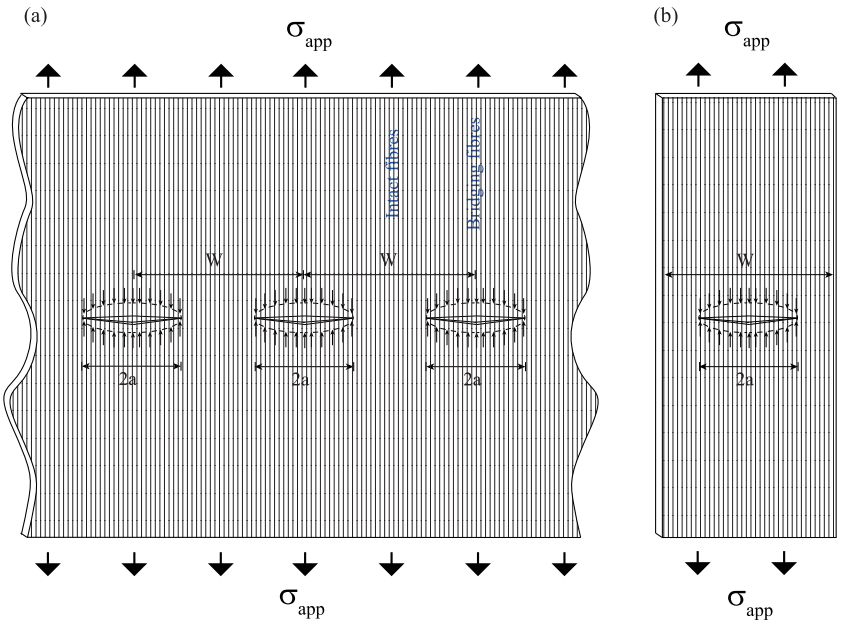

Fig. 3. An analogous comparison between (a) evenly distributed cracks in a FML panel and (b) a single crack in finite width FML panel.

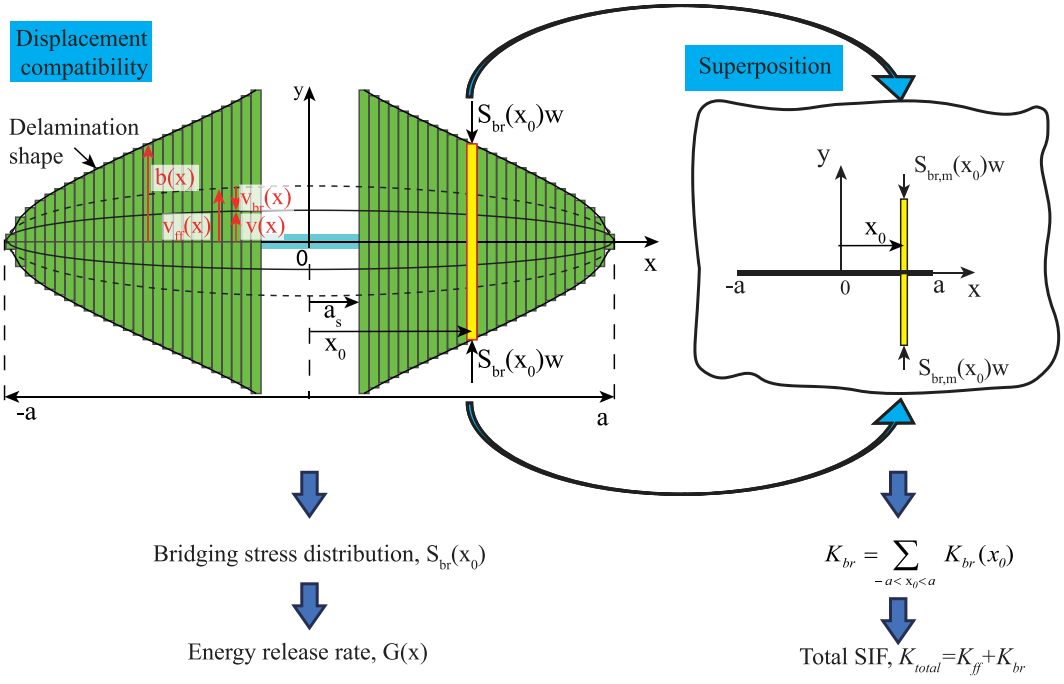

Fig. 4. Illustration of the displacement compatibility for calculating bridging stress distribution.

each bar element. Take the bar element at x as shown in Fig. 4, as an example, the displacement compatibility is expressed as:

$$\upsilon_{ff}(x) - \upsilon_{br}(x) = \delta_{ff}(x) + \delta_{pp}(x) \tag{4}$$

where υ_{ff} is the crack opening due to σ_m and the crack configuration while υ_{br} is the crack closing due to the bridging stresses, $S_{br}(x)$. δ_{ff} and δ_{pp} are the elongation over the delaminated length, $b(x)$, and the shear deformation of the bridging fibers.

A system of displacement compatibility equations have to be established for all the bar elements because $\upsilon_{br}(x)$ is not only a function of the bridging force at x, but also affected by other elements. It can be determined with the equation below:

$$\upsilon_{br}(x) = \sum_{-a<x_0<a} \upsilon_{br}(x, x_0) \tag{5}$$

The prepreg layer elongation, dependent on the bridging stress of the bar element at x, can be calculated by:

$$\delta_{ff}(x) = \frac{S_f + S_{br}(x)}{b(x)} \tag{6}$$

and the prepreg shear deformation δ_{pp} is independent of $S_{br}(x)$ but depends on σ_m and the laminate layup. Its expression can be found in [6].

The bridging stress distribution $S_{br}(x)$ can be determined by resolving the system of equations of displacement compatibility for all the bar elements as shown in Fig. 4, leading to the following equation:

$$S_{br}(x) = H^{-1}Q \tag{7}$$

with

$$H = \sum_{-a<x_0<a} \frac{v_{br}(x, x_0)}{S_{br}(x)} + \frac{b(x)}{E_f} \tag{8}$$

$$Q = v_{ff}(x) - \delta_{pp}(x) - \frac{S_f}{E_f} b(x) \tag{9}$$

The energy release rate distribution $G(x)$ can then be determined with the following equation [6,32]:

$$G(x) = \frac{n_f t_f}{2j E_f} \left(\frac{n_m t_m E_m}{n_m t_m E_m + n_f t_f E_f} \right) (S_f + S_{\mathrm{br}}(x))^2 \tag{10}$$

where the subscripts m and f represent the metal and fiber layers, respectively, while n and t denote the number and thickness of specific constituent layers within the fiber–metal laminates (FMLs). Additionally, j indicates the number of interfaces.

The principle of superposition is employed to determine K_{br} after the determination of the bridging stress distribution, $S_{br}(x)$, given in Eq. (11). The bridging forces of a bar element can be treated as symmetric point loads acting on a cracked plate and the corresponding SIFs at two crack tips can be determined based on the well-established solutions from the handbook [6,32].

$$K_{br} = \sum_{-a<x_0<a} K_{br}(x_0) \tag{11}$$

Substituting Eq. (11) into Eq. (3) leads to the total SIF K_{total} at the crack tip.

It is evident that K_{ff} and v_{ff} due to far-field applied loading are essential prerequisites for the fatigue analysis of the MSD scenario. The subsequent step is to determine the bridging stress distributions to obtain K_{br} and $G(x)$ for MSD cracks. The displacement compatibility between the multiple crack openings and the bridging fibers over numerous cracks need to be modeled [10].

The Westergaard stress functions are versatile in terms of calculating the stress intensity factor and crack opening displacement when a cracked 2D plate is under far-field applied loading or point loads. When the Westergaard stress function $Z_I(z)$ is known, the crack opening displacement along $y = 0$ can be determined as [44]:

$$v(x) = \frac{2}{E} \mathrm{Im}\{\tilde{Z}_I(x)\} \tag{12}$$

with $Z = \frac{d}{dz}\tilde{Z}$. The stress distribution ahead of crack tip along $y = 0$ can be determined with the equation below:

$$\sigma_{yy} = \mathrm{Re}\{Z_I(x)\} \tag{13}$$

Two approaches have been developed to deal with the interaction of evenly distributed multiple cracks in FMLs. They are detailed in the following respective subsections.

3.1. Approach 1

A direct method is adopted here, i.e., the stress intensity factor and the crack opening of evenly distributed multiple cracks in the metal layers owing to the applied far-field loading are calculated first. Subsequently, the crack opening due to the bridging fibers over multiple cracks is derived to implement the displacement compatibility. The resultant bridging stresses are further used to derive the bridging stress intensity factor and the energy release rate.

As a first step, the Westergaard stress function for the evenly distributed MSD scenario subjected to far-field loading, as shown in Fig. 5, is provided in the following equation [34,35].

$$Z_I(z)_{MSD} = \frac{\sigma_m}{\sqrt{1 - \sin^2\left(\frac{\pi a}{W}\right) / \sin^2\left(\frac{\pi z}{W}\right)}} \tag{14}$$

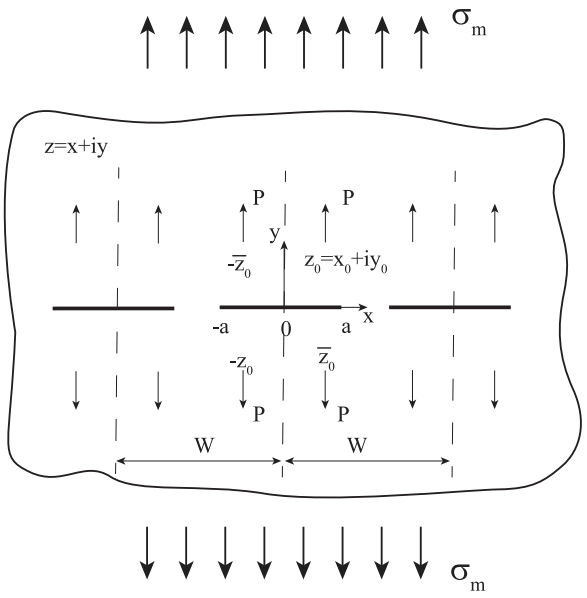

Fig. 5. Illustration of MSD cracks subjected to far-field stress and point loads. *Source:* Adapted from [34,35].

where $z = x + iy$ represents a point in the x-y coordinate system, with the origin located at the center of the crack and the x-axis aligned along the crack plane. The coordinate system is consistent with that in Fig. 4. σ_m is the lamina stress in the metal layers determined according to the classic laminate theory.

Based on Eq. (12), the crack opening displacement of multiple cracks under far-field applied loading, σ_m, can be given as:

$$v_{ff}(x) = \frac{2\sigma_m}{E\pi} W \cosh^{-1}\left(\frac{\cos\frac{\pi x}{W}}{\cos\frac{\pi a}{W}}\right) \tag{15}$$

The corresponding stress intensity factor, K_{ff}, can be calculated with Eq. (1). One should note that σ_{app} should be replaced by the stress in metal layers, σ_m. It is clear that the increases in the SIF and corresponding crack opening due to the presence of multiple collinear cracks are captured with Eq. (1) and (15).

What follows is the determination of the crack opening due to the bridging fibers and the implementation of displacement compatibility. It is assumed in this paper that the delamination size of each crack is identical and can be discretized into bar elements as shown in Fig. 4. Fortunately, the Westergaard stress functions for the MSD scenario subjected to symmetric point loads, illustrated in Fig. 6, have also been developed in the handbook [34,35]. Only $\bar{Z}_I(z)_{br}$ is of interest, which is provided in the following:

$$\begin{aligned}\bar{Z}_I(z)_{br} = \frac{P}{\pi}\left(1 - \alpha y_0 \frac{\partial}{\partial y_0}\right)\Bigg[&-\tan^{-1}\sqrt{\frac{\left(\cos\frac{\pi a}{W}/\cos\frac{\pi z}{W}\right)^2 - 1}{1 - \left(\cos\frac{\pi a}{W}/\cos\frac{\pi z_0}{W}\right)^2}} \\ &+ \tan^{-1}\sqrt{\frac{\left(\cos\frac{\pi a}{W}/\cos\frac{\pi z}{W}\right)^2 - 1}{1 - \left(\cos\frac{\pi a}{W}/\cos\frac{\pi \bar{z}_0}{W}\right)^2}} \\ &- \left(\tan^{-1}\frac{\sin\frac{\pi z_0}{W}\tan\frac{\pi z}{2W} - 1}{i\cos\frac{\pi z_0}{W}} - \tan^{-1}\frac{\sin\frac{\pi \bar{z}_0}{W}\tan\frac{\pi z}{2W} - 1}{i\cos\frac{\pi \bar{z}_0}{W}}\right)\Bigg]\end{aligned} \tag{16}$$

where

$$\alpha = \begin{cases} \frac{1}{2}(1+\nu) & \text{plane stress} \\ \frac{1}{2}\left(\frac{1}{1-\nu}\right) & \text{plane strain} \end{cases} \tag{17}$$

with $\nu = 0.3$ being the Poisson's ratio. For the analysis of the cracking the FMLs, the plane stress condition is normally chosen. It is noted that $y_0 = b(x_0)$, denoting the delamination length at x_0.

Substituting Eq. (16) into Eq. (12) can provide the crack opening, $v_{br}(x)$, due to the symmetric point loads as shown in Fig. 6. $v_{ff}(x)$ and $v_{br}(x)$ determined in this approach are substituted into Eq. (4) to calculate the bridging stress distribution, $S_{br}(x)$. It has to be pointed out that the bridging stress in the fiber layers has to be rewritten in terms of point loads in the metal layers in order to calculate the resultant crack opening displacement using the above equations:

$$P = S_{br} w \frac{n_f t_f}{n_m t_m} \tag{18}$$

After the bridging stress distribution is determined, K_{br} and $G(x)$ can be calculated. The stress intensity factor at the crack tip due to the symmetric point loads as depicted in Fig. 6 can be calculated using the following equation [34,35]:

$$K_{br}(x_0) = \frac{P}{W}\sqrt{W \tan\frac{\pi a}{W}}\left(1 - \alpha y_0 \frac{\partial}{\partial y_0}\right) \left\{ \frac{\cos\frac{\pi z_0}{W}}{\sqrt{\left(\sin\frac{\pi a}{W}\right)^2 - \left(\sin\frac{\pi z_0}{W}\right)^2}} + \frac{\cos\frac{\pi \bar{z}_0}{W}}{\sqrt{\left(\sin\frac{\pi a}{W}\right)^2 - \left(\sin\frac{\pi \bar{z}_0}{W}\right)^2}} \right\} \tag{19}$$

It is worth highlighting that Eq. (11) should be employed to determine K_{br} by substituting Eq. (19) back into Eq. (11). $G(x)$ is then determined according to Eq. (10).

In addition, to better illustrate the crack acceleration from the energy point of view as discussed in Section 2, it is worth understanding the stress/strain distribution ahead of the crack tip in the loading direction. The Westergaard stress function for MSD cracks subjected to far-field mode I loading can be used to determine the strain distribution in front of the crack tip in the loading direction:

$$\epsilon_{yy,MSD} = \frac{\sigma_m}{E_m\sqrt{1 - \frac{\sin^2(\frac{\pi a}{W})}{\sin^2(\frac{\pi x}{W})}}} \tag{20}$$

3.2. Approach 2

In contrast to the previous approach, Approach 2 adopts the assumption that the fatigue crack growth behavior of evenly distributed cracks in an FML is equivalent to that of a single crack in the FML with finite width, from the energy point of view. This assumption is visualized in Fig. 3 and has been discussed in Section 2. Although the effects of finite width on the fatigue crack growth behavior in an FML panel have been analyzed and an analytical model has been developed [43], the key aspects of this model are presented here for completeness and to better clarify the underlying assumption.

In order to aid in clarifying the effects of finite width on K_{total} and on the stress distribution ahead of the crack tip, the applied load, P_{app}, is decomposed as shown in Fig. 6. The loads transferred by the fibers over the crack, $P_{f,1}$, the fibers ahead of the crack, $P_{f,2}$, and the metal layers, P_m, can be easily determined using the lamina stresses in the metal layers σ_m and in the fiber layers S_f [43].

The total SIF accounting for the finite width effects is then given in Eq. (21) [43]. A correction factor, β, is directly applied to $K_{ff} = \sigma_m\sqrt{\pi a}$. The force equilibrium between the cracked cross-section and far-field, together with the Westergaard stress distribution, can be employed to determine β. The effects of finite width on K_{br} are analyzed by applying β to v_{ff} and subsequently calculating the resultant $S_{br}(x)$ and $f(\beta)K_{br}$ [43]. $f(\beta)$ cannot be explicitly given owing to the fact that Eq. (4) needs to be used to determine $S_{br}(x)$ and the SIF due to the bridging mechanism has to be integrated for $S_{br}(x)$. The same x-y coordinate system shown in Fig. 4 is used in this approach.

$$K_{total} = \beta K_{ff} + f(\beta)K_{br} \tag{21}$$

First, the determination of β is provided. For a single crack of $2a$ in an infinite plate, the Westergaard stress function is given in the following equation:

$$Z_I(z)_{single} = \frac{\sigma_m z}{\sqrt{z^2 - a^2}} \tag{22}$$

The stress distribution ahead of the crack can be determined by substituting Eq. (22) into Eq. (13); nevertheless, a correction factor β is needed to characterize the increase in the stress distribution when a finite width panel is concerned [39,43]. The strain distribution, given in Eq. (23), is preferred to the stress distribution because the iso-strain condition between the metal and fiber layers ahead of the crack tip is assumed. The loads transferred by the metal layers and fiber layers over the cross-section can then be easily calculated with the strain distribution given in Eq. (23).

$$\epsilon_{yy,single} = \frac{\beta\sigma_m}{E_m\sqrt{1 - (\frac{a}{x})^2}} \tag{23}$$

The implementation of the force equilibrium between the cross-section and the far-field, as shown in Fig. 6, is given by:

$$P_m + P_{f,2} = \int_a^{W/2}\left[\frac{\beta\sigma_m t_m n_m}{E_m\sqrt{1 - (\frac{a}{x})^2}} + \frac{\beta\sigma_m E_f t_f n_f}{E_m\sqrt{1 - (\frac{a}{x})^2}}\right] dx \tag{24}$$

The equation above can be resolved for β, which is expressed as:

$$\beta = \frac{t_m n_m W + E_f t_f n_f / E_m (W - 2a)}{\sqrt{W^2 - 4a^2(t_m n_m + E_f t_f n_f / E_m)}} \tag{25}$$

Consequently, the crack opening displacement accounting for the effect of the finite width is given as:

$$v_{ff}(x) = \frac{2\beta\sigma_m}{E_m}\sqrt{a^2 - x^2} \tag{26}$$

After knowing the crack opening displacement, Eq. (26) together with $v_{br}(x, x_0)$ established for a single crack subjected to symmetric point loads [32,43] need to be substituted into Eq. (4) in order to determine $S_{br}(x)$ that takes the effects of the finite width into consideration, as has been explained in the beginning of this section. The resultant $f(\beta)K_{br}$ can be determined following the established procedure [6,32,43]. $G(x)$ can also be determined according to Eq. (10).

3.3. Predicting crack growth and delamination propagation

Each approach described in the preceding subsections is capable of calculating K_{total} and $G(x)$ for a MSD configuration in an FML. Two Paris relations are employed to predict the fatigue crack growth rate and the delamination propagation rate respectively. The predicted results of the two approaches are verified and compared in Section 4.

The fatigue crack growth rate da/dN is modeled using an empirical Paris relation based on the effective SIF range at the crack tip:

$$\frac{da}{dN} = C_{cg}(\Delta K_{eff})^{n_{cg}} \tag{27}$$

where ΔK_{eff} accounts for the effect of stress ratio (R) on fatigue crack growth in monolithic metals. It is noted that R is defined as the ratio of $K_{total,min}$ under the minimum applied cyclic load to $K_{total,max}$ under the maximum applied cyclic load. ΔK_{eff} is further expressed as [6,32]:

$$\Delta K_{eff} = (0.55 + 0.33R + 0.12R^2)(1 - R)K_{total,max}. \tag{28}$$

The determined energy release rate G along the delamination front is used with another Paris relation for predicting the metal/composites interface delamination propagation rate, db/dN, which is provided in the following:

$$\frac{db}{dN} = C_d\left(\sqrt{G_{max}} - \sqrt{G_{min}}\right)^{n_d} \tag{29}$$

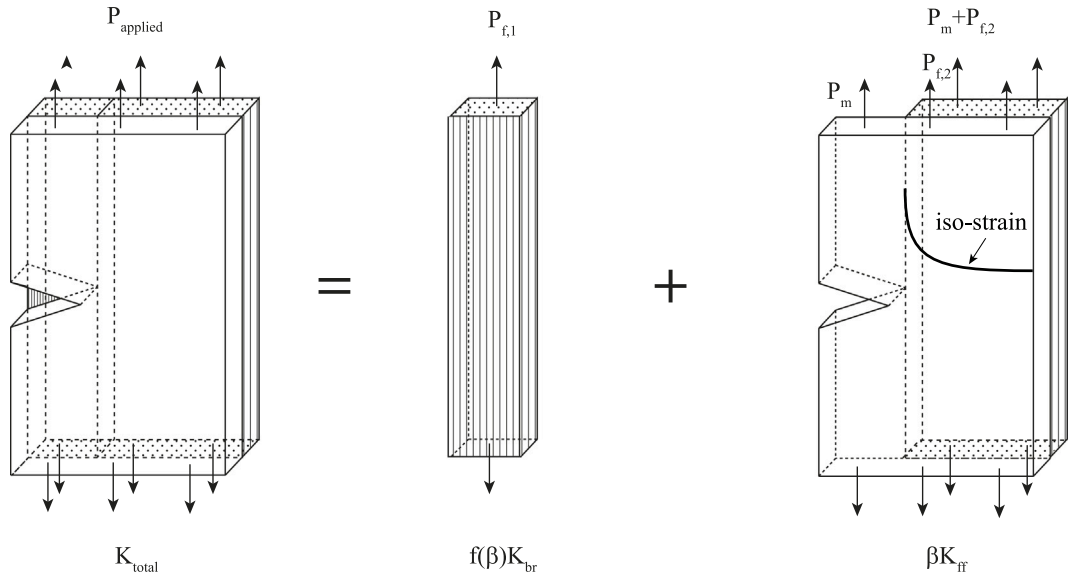

Fig. 6. Illustration of load decomposition for accounting for the finite width effects in FMLs.
Source: Adapted from [43].

where G_{max} and G_{min} represent the energy release rates under maximum and minimum applied cyclic loads respectively [6,32]. The Paris constants in Eqs. (27) and (29) for Glare, a typical variant of FML family, are: $C_{cg} = 2.17 \times 10^{-12}$, $n_{cg} = 2.94$, $C_d = 0.05$, $n_d = 7.5$ [6,32].

The crack length and corresponding delamination size are updated iteratively based on the predicted crack growth and delamination propagation rates for a given number of cycles. This process continues until the crack tips coalesce.

It is worth noting that the plastic zones ahead of the crack tips prior to coalescence can be empirically estimated using $K_{total,max}$. The crack growth calculation is terminated once the plastic zones coalesce to avoid the invalid application of linear elastic fracture mechanics (LEFM). However, neglecting the plastic zones introduces only negligible error in the predicted fatigue crack growth life, as the crack growth rate accelerates significantly prior to coalescence and the corresponding fatigue crack growth life is very short.

4. Model verification

The verification of the proposed models was carried out using published experimental results from some of the present authors [10]. Three Glare laminates containing MSD cracks were experimentally tested. Fig. 7 depicts the specimen configuration, with the central crack aligned with the specimen's center and two additional cracks located on the left and right sides, respectively. The Glare utilized consisted of alternating 2024-T3 aluminium sheets of 0.4 mm in thickness and S-2 glass fiber prepregs with FM 94 adhesive. Table 1 provides the test matrix and details of the specimen configuration. The specimen was tested under constant amplitude fatigue loading with the applied maximum stress, σ_{app}, provided in Table 1. The applied far-field stress ratio was $R = 0.05$. Crack lengths with corresponding fatigue lives were recorded during fatigue tests. The fatigue crack growth rate was calculated using the 7-point polynomial method following the ASTM E 647-00 standard [45]. The fatigue tests were terminated once two cracks coalesced. For more details of the test procedure, one is referred to Ref. [10].

It is worth noting that the crack spacing of $W = 30$ mm was adopted for analyzing the fatigue crack growth behavior in the tested specimens. However, the distance between the specimen edge and the neighboring crack center is 50 mm, which is much larger than $W/2 = 15$ mm. The effects of this discrepancy on the accuracy of the predicted results will be qualitatively discussed in the following from the energy point of view.

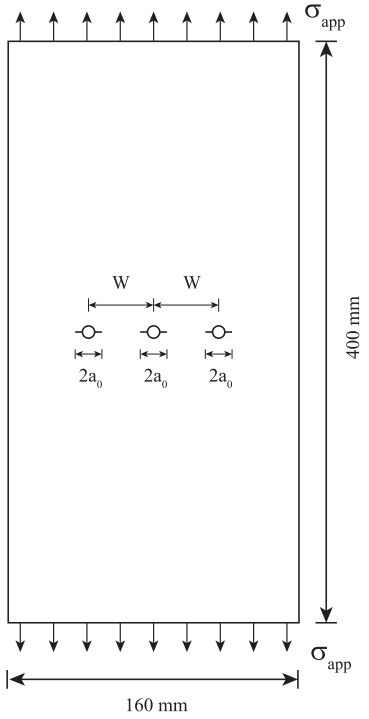

Fig. 7. Illustration of tested specimen configuration.

Table 1
Test matrix with details of the specimen configuration [10].

Specimen	n_m	n_f	Fiber direction	a_0 [mm]	W [mm]	σ_{app} [MPa]
Glare3-3/2-0.4	3	2	0/90	3	30	120
Glare4-3/2-0.4	3	2	90/0/90	3	30	100
Glare4-4/3-0.4	4	3	90/0/90	3	30	100

4.1. Fatigue life comparison

The predicted fatigue lives using the two proposed models in Section 3 are compared with the experimental results in Table 2. The prediction results from the previous model [10] are also compared. The

Table 2
Measured and predicted fatigue life comparison.

Specimen	Test results	MVF	Previous model		Approach 1		Approach 2	
			Pred.[a]	*R.E.*[b]	Pred.	R.E.	Pred.	R.E.
Glare3-3/2-0.4	74,000	0.69	51,600	−30.3%	68,872	−6.9%	72,119	−2.5%
Glare4-3/2-0.4	95,500	0.60	70,800	−25.9%	92,894	2.7%	96,104	0.6%
Glare4-4/3-0.4	104,000	0.57	83,400	−19.8%	104,165	0.2%	105,248	1.2%

[a] Prediction results.
[b] Relative error.

metal volume fraction (MVF) of each specimen is also provided in the table.

As can be seen, the two proposed models in this paper provide very close fatigue life predictions for all the tested FML configurations. In addition, the prediction accuracy of the two models has been greatly improved compared to the previous model developed in Ref. [10], with the relative error reduced from a range of −30.3% to −19.8%, to a much narrower range of −6.9% to 1.2%.

The predicted fatigue lives are in great agreement with the experimental results. The previous model treated the presence of MSD cracks as removal of metal strips which caused stiffness reduction and load redistribution to accelerate the fatigue crack growth [10]. This non-physical representation of cracks leads to overly conservative prediction results, the error in the prediction result is more pronounced for specimens with higher MVF value, see Table 2. In the current models, this non-physical representation of cracks is not adopted, the increase in crack opening and SIF due to the presence of MSD cracks are modeled in a manner closely reflects the reality. Consequently, the error in predicted fatigue lives is minimized independent of MVF values.

Another interesting observation from Table 2 is that Approach 1 predicts slightly shorter fatigue life than Approach 2. This is attributed to how the fibers ahead of the crack tips are treated in the prediction model. In Approach 1, the fibers ahead of the crack tips are not considered when determining the crack opening and SIF at the crack tip, whereas Approach 2 captures the effect of the fibers ahead of crack tips on the crack opening and SIF. From the energy point of view, the fibers ahead of the crack tips should also contribute to the load transfer and thus reduce the stress severity at the crack tip and corresponding crack opening [43]. This will be further examined in the following subsection.

4.2. Fatigue crack growth comparison

In addition to an overall comparison of the predicted and measured fatigue lives for all tested specimens, this section provides detailed comparisons of the predicted and experimental fatigue crack growth behavior, which are presented in Figs. 8–10. The markers in these figures represent the experimental results while lines represent prediction results. Figs. 8(a)–10(a) present the measured crack growth rates of the six crack tips of respective specimens and the predicted results. Figs. 8(b)–10(b) present the measured and predicted crack tip locations.

The predicted crack growth rates using the two approaches are compared against the experimental results. As can be seen from Figs. 8(a), 9(a) and 10(a), the prediction results from Approach 1 and Approach 2 closely align with each other and are in close agreement with the experimental results. Notably, the predictions overlap for shorter crack lengths. As crack length increases, the interaction and crack acceleration starts, the prediction models successfully capture this feature. As a result, only the a-N predictions from Approach 2 are compared against the measured ones, as shown in Figs. 8(b), 9(b) and 10(b), a high degree of overlap between the predicted and measured a-N curves can be observed.

Another observation is that the predictions from Approach 1 are marginally on the left side of those from Approach 2 when characterizing the crack acceleration, indicating that Approach 1 provides a slightly faster crack growth behavior, see Figs. 8(a) to 10(a). This discrepancy is attributed to the fact that the contribution of fibers ahead of the crack tips to the reduction in K_{ff} is not captured in Approach 1. Notably, Approach 2 effectively captures this mechanism through the implementation of Eq. (24). It demonstrates that, in addition to the bridging fibers reducing the crack growth rate, the fibers ahead of the crack tips also play a role in slowing down crack propagation.

Even though the predictions exhibit a fairly good degree of agreement with the experimental results, the predicted crack growth rates for the crack acceleration part are higher than experimental results, this is more pronounced in Fig. 8(a). As has been mentioned, the tested specimen is very wide, the distance between the specimen edge and the neighboring crack center is 50 mm, which is much larger than $W/2 = 15$ mm. As a result, the influence of free edges on crack acceleration for $a1$ and $a6$ is significantly smaller compared to that for the other crack tips, as can also be observed in the experimental results in Fig. 8(a). The redundant material in the tested specimens ahead of $a1$ and $a6$ contribute to the remaining cross-section area, reducing the increase in the stress distribution as the crack length increases. It is difficult to include the effects of the redundant material in the prediction model. This effect is more pronounced for specimens with higher MVF values, when comparing Figs. 8(a) to 9(a) and 10(a).

Overall, the proposed prediction models successfully capture the crack acceleration for the tested configurations. The predicted crack growth rate matches the experimentally obtained crack acceleration. The predicted and measured a-N curves show great agreement. It is noted that Approach 1 is cumbersome to implement as a series of complicated differential equations are involved while Approach 2 is much easier for engineering applications.

5. Conclusions

Two improved analytical models with a much higher prediction accuracy for analyzing MSD crack growth behavior in hybrid FML structures have been developed in this research. Compared to the previous analytical model, the accuracy has been significantly improved. The correlation between the predicted and experimental crack growth behavior is high. It is shown that the MSD crack growth behavior in FMLs can be analyzed in a manner analogous to that in monolithic plates. This approach allows for a simplified analysis framework, while delamination growth and crack propagation are addressed. The crack acceleration can be well captured by simplifying the MSD crack scenario into a single crack in a finite plate with the width equal to the spacing of cracks. The essence of this simplification lies in the fact that the energy dissipation dictates the crack growth behavior.

In comparison to fatigue cracking in monolithic plates, where only the finite width affects energy dissipation, the bonded elements ahead of the crack tip and the bridging elements over the crack are additional features that influence energy dissipation at the crack tip in bonded built-up structures. The contribution of the bonded elements ahead of the crack tip can be analyzed as part of the overall stiffness while the contribution of elements over the crack is analyzed through the bridging mechanism as a local crack shielding phenomenon. As a result, the simplified analysis of MSD in built-up structures cannot be analyzed by employing a correction factor. The intricate contribution of the stiffening elements ahead of the crack tip and the bridging elements to the crack growth behavior has to be precisely accounted for.

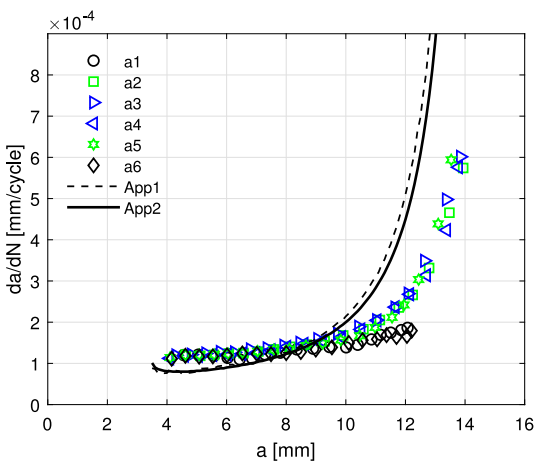

(a) Predicted and experimental da/dN comparison

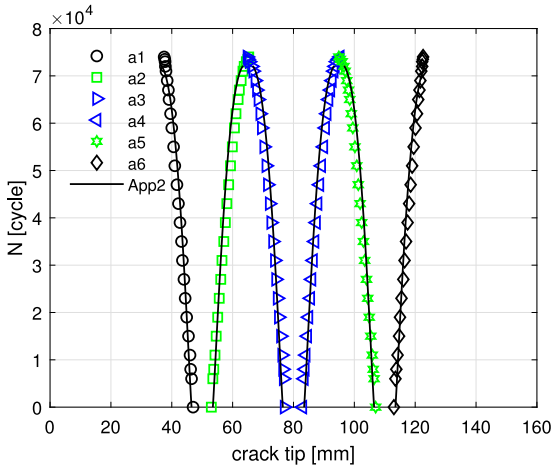

(b) Predicted and experimental a-N comparison

Fig. 8. Fatigue behavior prediction for Glare3-3/2-0.4 specimen.

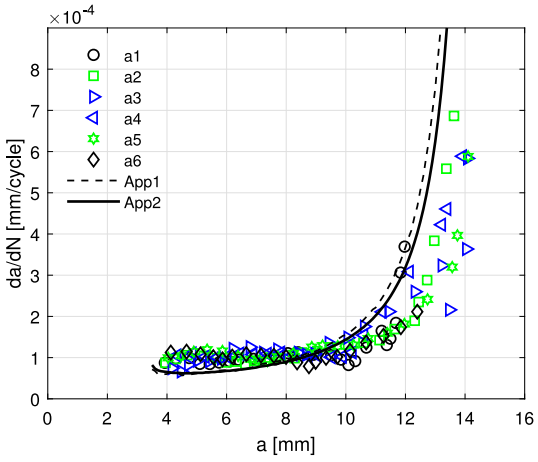

(a) Predicted and experimental da/dN comparison

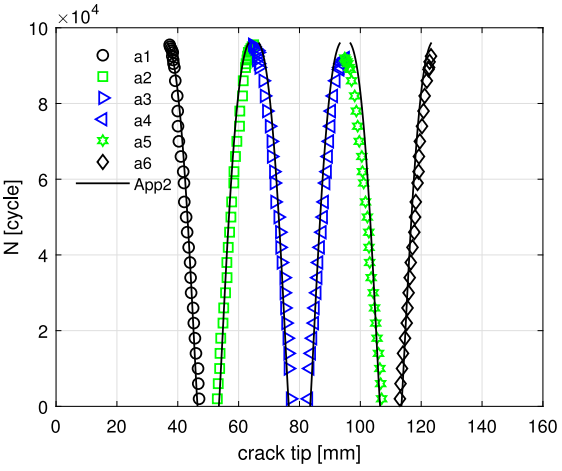

(b) Predicted and experimental a-N comparison

Fig. 9. Fatigue behavior prediction for Glare4B-3/2-0.4 specimen.

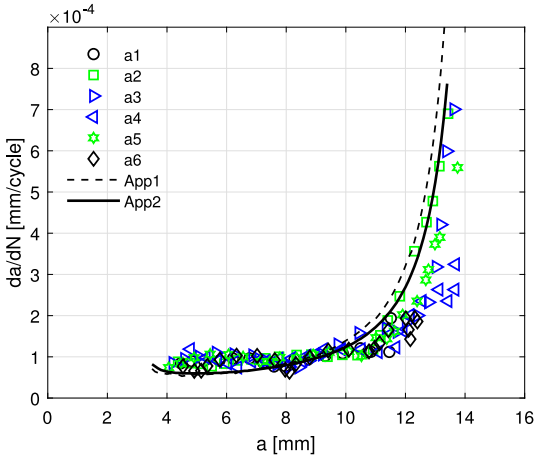

(a) Predicted and experimental da/dN comparison

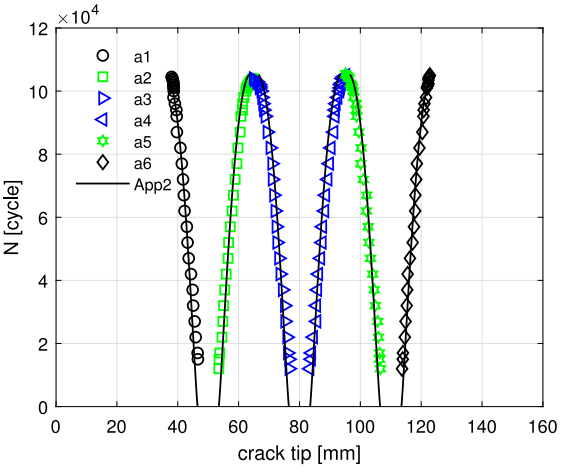

(b) Predicted and experimental a-N comparison

Fig. 10. Fatigue behavior prediction for Glare4B-4/3-0.4 specimen.

CRediT authorship contribution statement

Wandong Wang: Writing – original draft, Funding acquisition, Data curation, Conceptualization. **Hongchen Zhao:** Writing – review & editing, Visualization, Data curation. **Zhinan Zhang:** Validation, Methodology. **Wenbo Sun:** Writing – review & editing, Validation. **Calvin Rans:** Writing – review & editing, Validation, Data curation. **Yu'e Ma:** Writing – review & editing, Supervision, Project administration, Data curation.

Declaration of competing interest

The authors declare that they have no known competing financial interests or personal relationships that could have appeared to influence the work reported in this paper.

Acknowledgments

The financial funding from National Natural Science Foundation of China with the project number 52202509 is sincerely acknowledged.

Data availability

Data will be made available on request.

References

[1] Goranson U. Damage tolerance facts and fiction. In: International conference on damage tolerance of aircraft structures. Delft University of Technology; 2007.
[2] Jones R. Fatigue crack growth and damage tolerance. Fatigue Fract Eng Mater Struct 2014;37(5):463–83. http://dx.doi.org/10.1111/ffe.12155, https://onlinelibrary.wiley.com/doi/abs/10.1111/ffe.12155. https://onlinelibrary.wiley.com/doi/full/10.1111/ffe.12155.
[3] Meneghin I, Pacchione M, Vermeer P. Investigation on the design of bonded structures for increased damage tolerance. In: ICAF 2009, bridging the gap between theory and operational practice, Springer Netherlands; p. 427–47.
[4] Wang W, Zhou W, Ma Y, Motavalli M, Ghafoori E. Complete fatigue crack arrest in metallic structures using bonded prestressed iron-based shape memory alloy repairs. Int J Fatigue 2024;180:108104. http://dx.doi.org/10.1016/j.ijfatigue.2023.108104, URL https://www.sciencedirect.com/science/article/pii/S0142112323006059.
[5] Alderliesten RC, Homan JJ. Fatigue and damage tolerance issues of glare in aircraft structures. Int J Fatigue 2006;28(10):1116–23. http://dx.doi.org/10.1016/j.ijfatigue.2006.02.015.
[6] Alderliesten R. Analytical prediction model for fatigue crack propagation and delamination growth in glare. Int J Fatigue 2007;29:628–46.
[7] Vlot A. Glare history of the development of a new aircraft material. Dordrecht: Kluwer Academic; 2004.
[8] Ding Z, Wang H, Luo J, Li N. A review on forming technologies of fibre metal laminates. Int J Light Mater Manuf 2021;4(1):110–26. http://dx.doi.org/10.1016/j.ijlmm.2020.06.006, URL https://www.sciencedirect.com/science/article/pii/S2588840420300433.
[9] Ghiasvand S, Airoldi A, Bettini P, Mirani C. Analysis of residual stresses and interface damage propagation in hybrid composite/metallic elements monitored through optical fiber sensors. Aerosp Sci Technol 2022;129:107373. http://dx.doi.org/10.1016/j.ast.2022.107373, URL https://www.sciencedirect.com/science/article/pii/S1270963822000475.
[10] Wang W, Rans C, Benedictus R. Analytical prediction model for fatigue crack growth in fibre metal laminates with MSD scenario. Int J Fatigue 2017;104:263–72. http://dx.doi.org/10.1016/j.ijfatigue.2017.07.024, URL http://www.sciencedirect.com/science/article/pii/S0142112317303225.
[11] Eastin R. 'WFD' – what is it and what's 'LOV' got to do with it? Int J Fatigue 2009;31(6):1012–6. http://dx.doi.org/10.1016/j.ijfatigue.2008.04.003, http://www.sciencedirect.com/science/article/pii/S0142112308001084. http://ac.els-cdn.com/S0142112308001084/1-s2.0-S0142112308001084-main.pdf?_tid=e8630fd8-a86a-11e4-904f-00000aacb35d&acdnat=1422613964_a1a1d6cda51623109b4ad13d7167a192.
[12] Molent L, Dixon B. Airframe metal fatigue revisited. Int J Fatigue 2020;131:105323. http://dx.doi.org/10.1016/j.ijfatigue.2019.105323, URL https://www.sciencedirect.com/science/article/pii/S014211231930427X.
[13] Federal Register/Vol. 77, No. 101, Thursday May 24, 2012/ Rules and Regulations.
[14] Nesterenko B, Nesterenko G. Analysis of requirements on fatigue and damage tolerance for civil transport airplanes. In: Komorowski J, editor. 26th symposium of the international committee on aeronautical fatigue. Springer; p. 39–59.
[15] Schijve J. Fatigue of structures and materials. 2nd ed.. Dordrecht: Springer; 2008, ebrary http://site.ebrary.com/id/10275004. MyiLibrary http://www.myilibrary.com?id=195462. SpringerLink http://dx.doi.org/10.1007/978-1-4020-6808-9. SpringerLink http://springerlink.com/openurl.asp?genre=book&isbn=978-1-4020-6807-2.
[16] Schijve J. Crack stoppers and arall laminates. Eng Fract Mech 1990;37(2):405–21. http://dx.doi.org/10.1016/0013-7944(90)90050-Q, URL http://www.sciencedirect.com/science/article/pii/001379449090050Q.
[17] Rans C, Rodi R, Alderliesten R. Analytical prediction of mode I stress intensity factors for cracked panels containing bonded stiffeners. Eng Fract Mech 2013;97:12–29. http://dx.doi.org/10.1016/j.engfracmech.2012.11.001, URL http://www.sciencedirect.com/science/article/pii/S0013794412004341.
[18] Zhang X, Boscolo M, Figueroa-Gordon D, Allegri G, Irving PE. Fail-safe design of integral metallic aircraft structures reinforced by bonded crack retarders. Eng Fract Mech 2009;76(1):114–33. http://dx.doi.org/10.1016/j.engfracmech.2008.02.003, http://www.sciencedirect.com/science/article/pii/S0013794408000374. http://ac.els-cdn.com/S0013794408000374/1-s2.0-S0013794408000374-main.pdf?_tid=84b144c0-0898-11e6-871f-00000aab0f02&acdnat=1461336363_305f6e22d49c18085a85e0a3ca1e7804.
[19] Spronk S, Şen I, Alderliesten R. Predicting fatigue crack initiation in fibre metal laminates based on metal fatigue test data. Int J Fatigue 2014. http://dx.doi.org/10.1016/j.ijfatigue.2014.07.004, URL http://www.sciencedirect.com/science/article/pii/S014211231400187X.
[20] Zhang Z, Wang W, Rans C, Benedictus R. An experimental investigation into pin loading effects on fatigue crack growth in fibre metal laminates. Procedia Struct Integr 2016;2:3361–8. http://dx.doi.org/10.1016/j.prostr.2016.06.419, URL http://www.sciencedirect.com/science/article/pii/S2452321616304383.
[21] Khan SU, Alderliesten RC, Rans CD, Benedictus R. Application of a modified wheeler model to predict fatigue crack growth in fibre metal laminates under variable amplitude loading. Eng Fract Mech 2010;77(9):1400–16.
[22] Khan SU, Alderliesten RC, Benedictus R. Delamination in fiber metal laminates (GLARE) during fatigue crack growth under variable amplitude loading. Int J Fatigue 2011;33(9):1292–303.
[23] Tarpani ACSP, Barreto TA, Tarpani JR. Fatigue failure analysis of riveted fibre-metal laminate lap joints. Eng Fract Mech 2020;239:107275. http://dx.doi.org/10.1016/j.engfracmech.2020.107275, URL https://www.sciencedirect.com/science/article/pii/S0013794420308584.
[24] Galatolo R, Lazzeri R. Experiments and model predictions for fatigue crack propagation in riveted lap-joints with multiple site damage. Fatigue Fract Eng Mater Struct 2016;39(3):307–19.
[25] Wang HL, Grandt Jr AF. Fatigue analysis of multiple site damage in lap joint specimens. Report, American Society for Testing and Materials; 2000.
[26] Collins RA, Cartwright DJ. On the development of the strip yield model for the assessment of multiple site damage. Theor Appl Fract Mech 1996;25(2):167–78.
[27] Xu W, Wu XR. Weight functions and strip-yield model analysis for three collinear cracks. Eng Fract Mech 2012;85:73–87.
[28] Jin H, Zhang J, Shi S, Lei J, Shi L, Yang Y. Investigation on the interaction evolution and growth behavior of multiple cracks under fatigue loading. Theor Appl Fract Mech 2024;133:104559. http://dx.doi.org/10.1016/j.tafmec.2024.104559, URL https://www.sciencedirect.com/science/article/pii/S0167844224003094.
[29] Shen Z, Chen C, Xuan H, Quan C, Chen H, Zheng Y. Study on multiple fatigue cracks growth in the web of a hollow compressor impeller. Eng Fract Mech 2023;292:109582. http://dx.doi.org/10.1016/j.engfracmech.2023.109582, URL https://www.sciencedirect.com/science/article/pii/S0013794423005404.
[30] Wang W. Multiple-site damage crack growth behaviour in fibre metal laminate structures [Ph.D. thesis], Delft, the Netherlands: Delft University of Technology; 2017.
[31] Wang W, Rans C, Benedictus R. Theoretical analysis of fatigue failure in mechanically fastened fibre metal laminate joints containing multiple cracks. Eng Fail Anal 2018;91:151–64. http://dx.doi.org/10.1016/j.engfailanal.2018.03.012, http://www.sciencedirect.com/science/article/pii/S135063071830027X. https://ac.els-cdn.com/S135063071830027X/1-s2.0-S135063071830027X-main.pdf?_tid=fac05c2a-5389-4c29-b9a4-7b2ae2b0378e&acdnat=1551349224_b54157186d7118db641165e31b1ef8d0.
[32] Wang W, Rans C, Benedictus R. Analytical prediction model for non-symmetric fatigue crack growth in fibre metal laminates. Int J Fatigue 2017;103:546–56. http://dx.doi.org/10.1016/j.ijfatigue.2017.06.035, URL http://www.sciencedirect.com/science/article/pii/S0142112317302840.
[33] Wang W, Rans C, Alderliesten RC, Benedictus R. Predicting the influence of discretely notched layers on fatigue crack growth in fibre metal laminates. Eng Fract Mech 2015;145:1–14. http://dx.doi.org/10.1016/j.engfracmech.2015.06.062, http://www.sciencedirect.com/science/article/pii/S0013794415003288. http://ac.els-cdn.com/S0013794415003288/1-s2.0-S0013794415003288-main.pdf?_tid=223fa1e6-62bd-11e5-811f-00000aacb361&acdnat=1443100196_e58453b1056e3d208d2116871b0138b3.
[34] Tada H, Paris PC, Irwin GR. The stress analysis of cracks handbook. Hellertown: Del Research; 1973.
[35] Tada H, Paris PC, Irwin GR. The stress analysis of cracks handbook. 3rd ed.. Wiley; 2000.

[36] Isida M. Stress-intensity factors for the tension of an eccentrically cracked strip. J Appl Mech 1966;33(3):674–5. http://dx.doi.org/10.1115/1.3625138, http://appliedmechanics.asmedigitalcollection.asme.org/data/Journals/JAMCAV/25834/674_1.pdf.

[37] Dixon JR. Stress distribution around a central crack in a plate loaded in tension; effect of finite width of plate. J R Aeronaut Soc 1960;64(591):141–5. http://dx.doi.org/10.1017/S0368393100072266.

[38] Irwin G, Liebowitz H, Paris P. A mystery of fracture mechanics. Eng Fract Mech 1968;1(1):235–6. http://dx.doi.org/10.1016/0013-7944(68)90027-1, URL https://www.sciencedirect.com/science/article/pii/0013794468900271.

[39] Ravi Chandran K. Insight on physical meaning of finite-width-correction factors in stress intensity factor (K) solutions of fracture mechanics. Eng Fract Mech 2017;186:399–409. http://dx.doi.org/10.1016/j.engfracmech.2017.10.033, URL https://www.sciencedirect.com/science/article/pii/S0013794417310974.

[40] Wang W, Rans C, Benedictus R. Analytical solutions for crack opening displacements of eccentric cracks in thin-walled metallic plates. Thin-Walled Struct 2018;123:371–81. http://dx.doi.org/10.1016/j.tws.2017.11.047, URL https://www.sciencedirect.com/science/article/pii/S0263823117309783.

[41] Zhao Y, Alderliesten R, Zhou Z, Fang G, Zhang J, Benedictus R. On the physics of applying finite width and geometry correction factors in fatigue crack growth predictions of GLARE. Int J Fatigue 2018;117:189–95. http://dx.doi.org/10.1016/j.ijfatigue.2018.08.021, URL http://www.sciencedirect.com/science/article/pii/S0142112318303980.

[42] Zhao Y, Alderliesten R, Wu Z, Zhou Z, Fang G, Zhang J, et al. Determining finite-width-correction factors for fatigue crack growth prediction in GLARE using the equivalent compliance method. Int J Fatigue 2019;127:74–81. http://dx.doi.org/10.1016/j.ijfatigue.2019.05.037, URL http://www.sciencedirect.com/science/article/pii/S0142112319302294.

[43] Wang W. On the finite width correction factor in prediction models for fatigue crack growth in built-up bonded structures. Eng Fract Mech 2020;107156. http://dx.doi.org/10.1016/j.engfracmech.2020.107156.

[44] Tada H, Ernst HA, Paris PC. Westergaard stress functions for displacement-prescribed crack problems—I. Int J Fract 1993;61(1):39–53. http://dx.doi.org/10.1007/BF00032338.

[45] ASTM. Standard test method for measurement of fatigue crack growth rates. ASTM E647-00, West Conshohocken, PA: American Society for Testing and Materials; 2000.